Journal of Magnetic Resonance 260 (2015) 20–27

Contents lists available at ScienceDirect

Journal of Magnetic Resonance

journal homepage: www.elsevier.com/locate/jmr

Communication

High-throughput hyperpolarized ^{13}C metabolic investigations using a multi-channel acquisition system

Jaehyuk Lee [a], Marc S. Ramirez [a], Christopher M. Walker [a], Yunyun Chen [b], Stacey Yi [a], Vlad C. Sandulache [c], Stephen Y. Lai [b], James A. Bankson [a,*]

[a] Department of Imaging Physics, The University of Texas M.D. Anderson Cancer Center, Houston, TX, USA
[b] Department of Head & Neck Surgery, The University of Texas M.D. Anderson Cancer Center, Houston, TX, USA
[c] Department of Otolaryngology, Baylor College of Medicine, Houston, TX, USA

ARTICLE INFO

Article history:
Received 10 April 2015
Revised 27 August 2015
Available online 5 September 2015

Keywords:
Dynamic nuclear polarization
Hyperpolarization
^{13}C spectroscopy
Hyperpolarized pyruvate
Cancer
Multichannel spectroscopy
Dynamic spectroscopy
Coil array

ABSTRACT

Magnetic resonance imaging and spectroscopy of hyperpolarized (HP) compounds such as [1-^{13}C]-pyruvate have shown tremendous potential for offering new insight into disease and response to therapy. New applications of this technology in clinical research and care will require extensive validation in cells and animal models, a process that may be limited by the high cost and modest throughput associated with dynamic nuclear polarization. Relatively wide spectral separation between [1-^{13}C]-pyruvate and its chemical endpoints *in vivo* are conducive to simultaneous multi-sample measurements, even in the presence of a suboptimal global shim. Multi-channel acquisitions could conserve costs and accelerate experiments by allowing acquisition from multiple independent samples following a single dissolution. Unfortunately, many existing preclinical MRI systems are equipped with only a single channel for broadband acquisitions. In this work, we examine the feasibility of this concept using a broadband multi-channel digital receiver extension and detector arrays that allow concurrent measurement of dynamic spectroscopic data from *ex vivo* enzyme phantoms, *in vitro* anaplastic thyroid carcinoma cells, and *in vivo* in tumor-bearing mice. Throughput and the cost of consumables were improved by up to a factor of four. These preliminary results demonstrate the potential for efficient multi-sample studies employing hyperpolarized agents.

1. Introduction

The relatively high sensitivity and natural abundance of ^{1}H nuclei in the body permit noninvasive morphological and functional investigation of disease with magnetic resonance (MR) imaging (MRI) and spectroscopy (MRS). The excellent chemical specificity of MR further enables assessment of certain biochemical characteristics of tissue. It is well-known, for example, that many malignancies undergo higher levels of glycolysis and lactic acid fermentation despite normal tissue oxygenation, a condition that is often referred to as aerobic glycolysis or the Warburg effect [1,2]. Therefore, dynamic changes in pyruvate and lactate levels *in vivo* could serve as useful biomarkers of cancer metabolism. The unique ^{13}C spectroscopic signatures of pyruvate and lactate could permit their non-invasive observation through MRS, MRI, and MR spectroscopic imaging (MRSI), though such measurements have low sensitivity due to low natural abundance (~1%) and a gyromagnetic ratio that is one-quarter that of ^{1}H. Low sensitivity necessitates prohibitively long scan times for signal averaging, rendering the use of ^{13}C signal from endogenous metabolites impractical for real-time measurement of metabolism *in vivo* [3].

To overcome sensitivity limitations, methods that create a hyperpolarized (HP) nuclear spin population may be used to dramatically enhance the signal of exogenous substrates. One such method, known as dissolution dynamic nuclear polarization (DNP), involves combining an enriched substrate with a polarizing radical, and transferring polarization from unpaired electrons to nuclear spins through microwave radiation at very low temperatures [4,5]. The HP sample is rapidly dissolved with a heated buffer solution and quickly transferred to the MR scanner, where it may be used to perform experiments with greater than 10,000-fold signal enhancement [5]. Preliminary studies involving HP [1-^{13}C]-pyruvate include very promising investigations of real-time cancer metabolism in cells [6,7], cancer diagnosis and staging [8,9],

* Corresponding author at: Department of Imaging Physics, The University of Texas M.D. Anderson Cancer Center, 1515 Holcombe Blvd, Unit 1902, Houston, TX 77030, USA.
E-mail address: jbankson@mdanderson.org (J.A. Bankson).

http://dx.doi.org/10.1016/j.jmr.2015.08.025
1090-7807/

therapeutic response [10–19], and detection of cardiac metabolism [20,21].

Although HP ^{13}C MR shows great potential for *in vitro* and both preclinical and clinical studies *in vivo*, it is not without drawbacks. In addition to the technical challenges for HP data acquisition, which are confounded by T_1 relaxation and nonrenewable signal loss due to radiofrequency (RF) excitation, several practical limitations associated with cost, time, and efficiency may delay the widespread preclinical use of HP MRI. First, DNP requires significant build-up time to reach the desired polarization: ~45 min to reach 90% of the maximum polarization level for [1-^{13}C] pyruvate, limiting the number of observations that can be made in a given interval of time. Second, costs associated with the radical and the ^{13}C-enriched substrate can be significant. Third, the DNP process proceeds most efficiently at very low temperature ~1.4 K, requiring the use of cryogens that must often be replenished. System maintenance alone represents a large fraction of the overall cost. In addition, only on the order of 5% of the total dissolution volume may be used for *in vivo* studies in mice, and a smaller fraction may be used *in vitro* to maintain a physiologically relevant concentration in cell studies, resulting in substantial waste [22]. More efficient use of HP ^{13}C agents would reduce cost and facilitate integration of this technology into routine biomedical research.

Although the vast majority of preclinical MR systems are equipped with no more than one channel which may be used for detection of ^{13}C signals, a handful of clinical scanners support multi-channel HP ^{13}C acquisition. These receivers, in combination with RF coil arrays, have permitted improved sensitivity [23,24], increased spatial coverage [25], and a means to perform partially parallel imaging [26].

To improve the efficiency of *ex vivo*, *in vitro*, and *in vivo* preclinical experiments involving HP ^{13}C, we have implemented a low-cost, multi-channel, broadband RF receiver with various array coils for performing multiple measurements in parallel. Signal-to-noise ratio (SNR) calculations, based on data acquired from an enriched ^{13}C urea phantom at thermal equilibrium, were used to evaluate consistency among channels and to compare performance against standard scanner hardware. The capability to simultaneously capture spectral dynamics from four distinct volumes was established using a 4-channel RF coil array and phantoms that contained varying concentrations of enzyme infused with HP [1-^{13}C] pyruvate. High-throughput *in vitro* experiments, involving human thyroid cancer cells, were then performed with a dual Helmholtz coil to demonstrate the feasibility for improving measurement efficiency while preserving experimental and environmental consistency. Finally, two surface coils were placed over distinct subcutaneous tumors on one mouse, to demonstrate simultaneous *in vivo* measurement of metabolism from separate and distinct anatomic sites. This establishes a platform where paired examination of experimental therapies may be readily and rapidly performed, with reduced deviation due to biological or experimental variations.

2. Materials and methods

2.1. Multi-channel receiver

The home-built receiver system includes an RF module, a power supply module, an analog-to-digital conversion (ADC) acquisition board, and a Linux workstation. The RF module contains four RF channel cards, each supporting four independent receive channels, and a local oscillation (LO) signal distribution card. The LO signal is derived from the MRI console or alternatively provided by an external signal generator, and it provides a reference for down-converting the input RF signal to the baseband output. Baseband signals were acquired through a high speed ADC board (ICS-645D, Gloucester, Ontario, Canada) that was controlled by the Linux workstation. The ADC board is capable of processing streams from up to 32 channels simultaneously, although 16 channels are currently implemented. The digitized data was processed and visualized on the workstation.

The RF module was built using a nuclear instrument module (NIM) system bin (4001C, ORTEC, Oak Ridge, TN), which includes a backplane with several dedicated pins for supplying power to each bin and the circuit boards they contain. An XLC01 (Excelsys, Rockwall TX) power source provides stable 6 V and 12 V signals. All electronics were assembled on an FR4 circuit board (thickness 0.059″, 1 oz copper, LPKF, Garbsen, Germany). Circuit layouts were drawn with Cadence (v16.3) software and manufactured using a ProtoMat C100/HF (LPKF, Garbsen, Germany) milling machine.

Summary diagrams for one 4-channel RF board are shown in Fig. 1. Signal levels must be carefully managed for good conversion without distortion or addition of excessive noise. The local LO distribution circuit (Fig. 1A) requires a 13.5 dBm signal at its input; we used an ADL5601 (Analog Devices, Norwood, MA) amplifier to achieve the correct signal amplitude. After the LO signal is divided using a four-way splitter (PSC-4-1W+, Mini-Circuits, Brooklyn, NY), it is distributed to each of the four receive channels (Fig. 1B) on that board. Two gain stages (RAM-6+ and MAR-1SM, Mini-Circuits) on the receive boards provide ~35 dB of gain that for the MR signal path that can be adjusted using a voltage-controlled attenuator (G-1, Macom, Lowell, MA). Conversion from RF to baseband is performed with a TUF-3+mixer (Mini-Circuits). Two series low-pass filters with ~830 kHz cut-off frequency (LPF-B0R6, Mini-Circuits) are used for anti-aliasing and noise rejection, and finally, a driver amplifier (OPA843, Texas Instruments, Dallas, TX) maximizes the dynamic range of the ADC and a cross-diode pair (HSMP-3892, Avago Technologies, San Jose, CA) protects the ADC board from any potentially damaging high-voltage signals.

The SNR of the receiver, including the analog path and digital signal processing, was compared to the 7T Biospec MRI system by scanning a 2 mL phantom with 8 M ^{13}C-urea at thermal equilibrium. The output signal from the preamplifier was split two ways and simultaneously fed to the console receiver and to each of four channels from the multichannel receiver in turn. A pulse-acquire sequence (TR = 2000 ms, TE = 2.6 ms, 2048 readout points, BW = 4.96 kHz, 45° excitation angle, and 96 repetitions) was used for data collection. SNR was calculated by dividing the temporal mean of the phase-corrected real component of the urea peak (integrated over the full spectral width) by the standard deviation of a noise-only region.

2.2. Coil design

RF array coils were designed, built, and tested in-house. Advantages of surface coils include high local sensitivity, spatial localization, and flexibility of positioning. For the *ex vivo* experiments with enzyme phantoms, a four-channel surface coil array was implemented to measure four samples simultaneously. Each coil consisted of a single loop (outer diameter (OD) = 7 mm, inner diameter (ID) = 4.5 mm) with tuning and matching capacitors, and coil centers were positioned to correspond with four wells of a standard 96-well plate, in a 2×2 grid arrangement, with 20 mm separation between nearest coils. Inductive coupling between neighboring coils, as measured on a network analyzer (4395A; Agilent Technology, Santa Clara, CA), was between −34.8 dB and −35.7 dB at 75.53 MHz.

In vitro experiments to characterize tumor cell metabolism using HP-[1-^{13}C]-pyruvate were performed using an array of two identical Helmholtz coils (10 mm ID), illustrated in Fig. 2. Coils were separated by 80 mm center-to-center and the inductive coupling between them was −31.4 dB at 75.53 MHz. The SNR of this

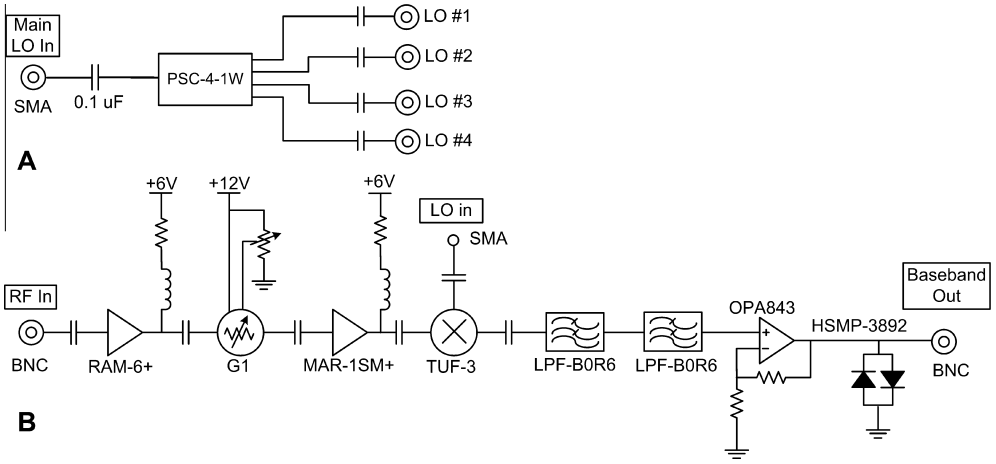

Fig. 1. Schematics of the multichannel receiver boards. (A) Local oscillator distribution – the LO is amplified and distributed to each RF channel. (B) RF channel card – the RF signals from various MRI coils are amplified and converted to baseband signals, then digitized using the Analog-to-Digital converter in the Linux workstation for subsequent digital signal processing.

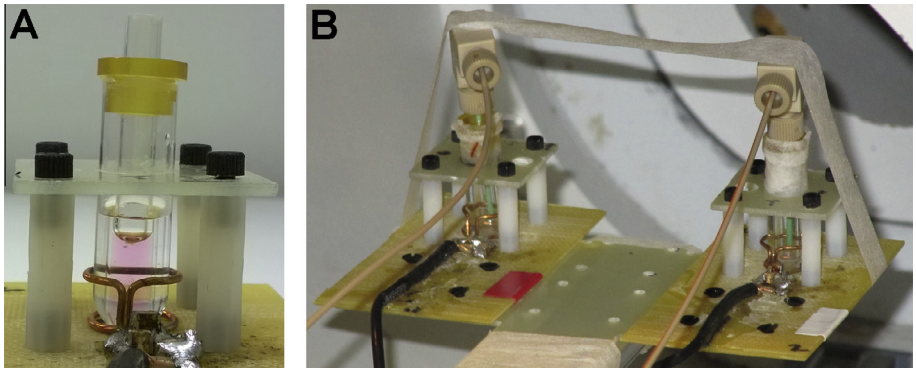

Fig. 2. Two-channel array of Helmholtz coils. (A) Nested 5 mm and 10 mm NMR tubes fit just within the Helmholtz coil. The space between NMR tubes is filled with water to remove the susceptibility interface from the region of interest inside the interior tube. (B) Two independent coils are fixed to a structure that fits within the larger transmit coil (72 mm ID).

Helmholtz coil array, including the home-built passive Tx/Rx switch and a preamplifier (MicroWave Technology Inc, Fremont, CA), was compared to the each coil located at isocenter by scanning a 250 μL phantom containing 8 M ^{13}C-urea at thermal equilibrium.

For the *in vivo* experiment, two 15-mm ID dual-turn surface coils were similarly implemented for placement on distinct tumor sites. Interactions between transmit and receive coils was minimized by active decoupling, using a PIN diode switch under control of console electronics. Geometric decoupling between surface coils depends on the particular tumor locations, but efforts were made to place coils orthogonal to each other. Low input impedance preamplifiers provided up to an additional ~15 dB of isolation [27,28].

2.3. Dynamic nuclear polarization

Hyperpolarized pyruvate was prepared using a mixture of 6.5–26 mg of neat [1-^{13}C] pyruvic acid (Isotech Sigma–Aldrich, St. Louis, MO) containing 15 mM OX063 trityl radical (GE Healthcare, Amersham, Denmark) and 1.5 mM aqueous solution of a gadolinium chelate (ProHance, Bracco Diagnostic, Singen, Germany) [5]. The ^{13}C-labeled sample was polarized by DNP using a Hypersense system (Oxford Instruments, Abingdon, UK). The sample was inserted into a 3.35 T vertical bore magnet, frozen to 1.4 K, and irradiated at 94.12 GHz for approximately 45 min.

After a plateau in the solid-state polarization level was reached, the frozen sample was rapidly dissolved using a 4 mL buffer solution at 180 °C containing 40 mM TRIS (7.6 pH preset), 20–80 mM NaOH, 0.1 g/L EDTA, and 50 mM NaCl. The final solution, containing 20–80 mM [1-^{13}C] pyruvate, was flushed into a large syringe near the magnet and the appropriate volume was drawn and administered for scanning.

2.4. MR signal acquisition and data analysis

All experiments were performed on a 7 T Biospec small animal MRI scanner (Bruker Biospin MRI, Billerica, MA) equipped with a single channel for carbon excitation/reception and gradients with a 12-cm ID. A dual-tuned ^{1}H/^{13}C birdcage coil with 72-mm ID (1P T10334, Bruker Biospin MRI, Inc., Ettlingen, Germany) was used for acquiring ^{1}H reference images. Dynamic HP ^{13}C spectroscopic data were also acquired through the broadband multichannel receiver extension, which was triggered by a TTL output signal from the Biospec. For ^{13}C, the birdcage coil was used for transmission and the appropriate surface coil array was used for signal reception.

All data reconstruction and analyses were performed using Matlab (The MathWorks Inc., Natick, MA). The dynamic spectra were phase-corrected and line broadening was applied. Spectral information centered at the 75.53 MHz ^{13}C Larmor frequency was mixed down to a sequence-dependent intermediate frequency

(IF). The analog signal was then sampled and converted into a complex signal at baseband by digital I/Q demodulation. A 2 MHz sampling rate was selected to ensure Nyquist sampling of the full bandwidth of the low pass filters (f_c ~830 kHz). This avoided not only signal aliasing, but also aliasing of noise in the passband of the low pass filters. The signal was then filtered with a finite-impulse-response (FIR) filter, and data were decimated to the final signal length and bandwidth, then transformed by Fast-Fourier-Transform (FFT) for analysis and display in the spectral domain. The area under the real spectral peaks for pyruvate and lactate were integrated over full-width at half-maximum, and integrated again over time to calculate total signal from each metabolite. The normalized lactate (nLac) ratio was calculated as lactate divided by the sum of pyruvate and lactate signals.

2.5. Enzyme phantom experiment

Four 300 μL wells of a standard 96-well plate were filled with an enzyme mixture containing 4.6 mM β-NADH (Sigma Aldrich), a variable concentration (0.0, 1.0, 3.0, and 9.0 U/mL) of lactate dehydrogenase (LDH) (Worthington Biochemical Corp., Lakewood, NJ), and 4 mM final concentration of HP [1-^{13}C] pyruvate in a buffer solution containing 203.3 mM NaCl and 81.3 mM Tris (7.6 pH preset). NADH and LDH were thawed from fresh aliquots that were stored at −80 °C [29]. The HP pyruvate was mixed with other reagents outside the magnet bore and immediately moved to the magnet isocenter, after which a pulse-acquire scan (TR = 2000 ms, TE = 2.4 ms, 2048 readout points, 4.96 kHz BW, 15° flip angle, 96 repetitions) was initiated. Data were apodized by a 15 Hz exponential window.

2.6. Cell experiments

Highly aggressive HTH-83 human anaplastic thyroid carcinoma (ATC) cells were cultured at 37 °C in a humidified atmosphere consisting of 95% air and 5% CO_2 with 80–90% confluence of 10 × 15 cm dishes. Cells were treated with 5 mM 2-deoxyglucose (2-DG) (Sigma) for 1 h then harvested for experiments. Control cells and 2-DG treated cells were adjusted to the same concentration (4.5×10^7 cells/mL) before imaging. A portion of the cell suspension was mixed with 0.4% Trypan blue solution (Hyclone) at a 1:1 ratio for 5 min at room temperature. Cell viability was measured using an Automatic Cellometer Reader (Nexcelom, MA). Cells demonstrated excellent viability in both control (96.1%) and 2-DG (97.5%) groups.

To assess the impact of 2-DG on cancer cell metabolism, control and 2-DG treated cells were simultaneously probed with HP-pyruvate. Concentric 5 mm and 10 mm NMR tubes (Wilmad-Labglass, Vineland, NJ) were placed vertically in the Helmholtz coils (see Fig. 2A), and the space between NMR tubes was filled with water to facilitate placement, shimming, and removal of the air/water susceptibility interface from the test solutions. After dissolution, approximately 12.5 μL of 20 mM HP-pyruvate was pipetted into the tip of each 1 mL syringe containing 510 μL of cell slurry. Approximately 250 μL of the suspensions (1.1×10^6 cells) were delivered through 1 m PEEK tubing (Restek Co., Bellefonte, PA) that led from the edge of the bore to the coils at isocenter. The mixture contained final concentrations of ~1 mM HP [1-^{13}C] pyruvate and ~0.5 mM unlabeled lactate. A slice-selective pulse sequence (TR = 2000 ms, TR = 2.4 ms, 2048 readout points, 4.96 kHz BW, 15° flip angle, 96 repetitions) was initiated by the HyperSense system at the beginning of dissolution. 15 Hz line broadening was applied.

2.7. In vivo multi-tumor measurements

In some experiments, it is possible to achieve multiple experimental conditions within a single animal. Different doses of radiation therapy could be simultaneously administered, for example, to two or more tumors that were implanted within a single experimental animal. Thus, the ability to collect independent and localized metabolic information from different anatomic regions could reduce experimental variations, allow the use of paired statistical tests with higher power, and lower the number of animals that are required in order to detect statistically significant differences.

Athymic nude mice were used to demonstrate simultaneous multi-volume HP ^{13}C MRS *in vivo* on a single animal. Luciferase-tagged 0805C ATC cells were implanted into opposing flanks two weeks before imaging. Prior to experimentation, an animal was anesthetized by isoflurane inhalation (2% in oxygen) and placed supine on a mouse sled with isoflurane supplied through a nose cone. Body temperatures were maintained at ~37 °C by circulating warm water through the sled. Respiratory rate and body temperature were closely monitored with a small-animal monitoring system (Small Animal Instruments, Inc., Stony Brook, NY). Following anatomic ^{1}H imaging, a 10-mm axial slice that contained both tumors was prescribed. 200 μL of 80 mM HP [1-^{13}C] pyruvate solution was injected via tail vein. Dynamic spectra were acquired using a slice-selective pulse acquire ^{13}C sequence (TR = 1500 ms, TE = 2.4 ms, 2048 readout points, 4.96 kHz BW, 15° flip angle, 120 repetitions). All procedures were approved by our Institutional Animal Care and Use Committee, which is accredited by the Association for the Assessment and Accreditation of Laboratory Animal Care International.

3. Results

3.1. SNR performance

Measurements from the 2 mL, 8 M ^{13}C urea phantom at thermal equilibrium reveal that comparable SNR values are observed through the multi-channel receiver extension and the Biospec receiver. The paired SNR results are listed in Tables 1 and 2. The slightly higher average SNR in the multi-channel receiver (1.50×10^4 vs. 1.13×10^4) may be explained by imbalance in the splitter, differences in cable length and routing, and differences in gain and digital signal processing algorithms in the two systems. There was a larger variation among SNR measurements performed on the multi-channel receiver compared to the console receiver, likely reflecting relatively minor differences in components along the signal path in the home-built receiver.

Signal degradation due to suboptimal global shim is a significant concern for multi-volume MRS. SNR from was measured from 250 μL aliquots of 8 M ^{13}C-urea to assess the impact of simultaneous offset measurements using the 2-channel Helmholtz array compared to single-channel measurements at with each coil at isocenter. Table 2 shows a slight degradation of less than 5% (2.07×10^3 vs 2.16×10^3) in SNR for the simultaneous/offset case.

Table 1
SNR of Biospec receiver and each channel of one RF board from the broadband receiver extension.

Receiver Channel	Multi-channel	Biospec
Channel #1	1.5112×10^4	1.1256×10^4
Channel #2	1.5228×10^4	1.1251×10^4
Channel #3	1.4932×10^4	1.1296×10^4
Channel #4	1.4604×10^4	1.1250×10^4
Mean	1.4969×10^4	1.1263×10^4
Std Dev	2.7211×10^2	2.1991×10^1

Table 2
SNR of Helmholtz coils at isocenter and on dual-coil array setup.

Coil	Array setup (offset) SNR	Individual coils (isocenter) SNR
Helmholtz #1	1.96×10^3	2.05×10^3
Hemlholtz #2	2.18×10^3	2.27×10^3
Mean	2.07×10^3	2.16×10^3

Linewidths were not significantly increased in the multi-coil configuration compared to coils placed at isocenter (0.5 ppm vs 0.8 ppm) and were in all cases sufficient for analysis due to the wide chemical shift spacing for [1-^{13}C]-pyruvate and its chemical endpoints *in vivo*.

3.2. Four channel test with enzyme phantoms

The feasibility of independent multi-channel dynamic acquisitions was initially demonstrated by scanning multiple enzyme phantoms simultaneously. Fig. 3 shows that each channel presented different nLac values that were proportional to LDH concentration. The nLac values were 0.12 for channel 2, 0.48 for channel 3, and 0.76 for channel 4. No lactate production was expected or observed in channel 1 (nLac = 0) because this control case did not include the necessary enzyme. There is no evidence of coupling from the strong lactate signal in channels 3–4 into channel 1.

3.3. Thyroid cancer cell experiment

Multichannel cell experiments were performed to investigate the feasibility of high-throughput HP ^{13}C experiments using a small volume (~250 μL) of cells. In this experiment, differences in the conversion of HP pyruvate to lactate were compared in control cells and those exposed to 2-DG. Fig. 4 shows the different normalized signal intensity of HP ^{13}C pyruvate and lactate produced by the cells. In this experiment, the result indicates distinctive nLac values between two channels: 0.28 for the treated cells measured through channel 1 and 0.45 for the untreated cells measured with channel 2. These results are consistent with prior literature; 2-DG is a competitive inhibitor of glycolysis, and it has been shown to reduce the conversion of HP pyruvate to lactate by lowering intracellular reducing potential [30].

3.4. Animal model experiment using a dual-coil

To explore the potential for paired tumor measurements while minimizing biological and environmental variations between groups, we investigated the utility and feasibility of simultaneous multi-volume HP ^{13}C MRS *in vivo*. To confirm correspondence between acquisition through the multi-channel and standard receivers, the amplified signal from coil 1 (located over tumor 1) was split between the standard console receiver and the multi-channel receiver. The amplified signal from coil 2 (sensitive to tumor 2) was directly fed to a second channel of the multi-channel receiver. Fig. 5 shows signal from the injected HP [1-^{13}C] pyruvate and its conversion into HP lactate. The spectral data were also summed over time to generate cumulative spectra of the HP metabolites (Fig. 6). These spectra demonstrate distinct tumor metabolism and the consistency of data quality acquired through the standard receiver and the broadband receiver extension developed in this work.

4. Discussion

In this work, we have demonstrated the versatility of simultaneous multi-sample HP ^{13}C MR experiments made feasible by a broad-band multi-channel receiver extension and multinuclear array coils. Various responses to HP [1-^{13}C] pyruvate were demonstrated in controlled enzyme phantoms *ex vivo*, cancer cells *in vitro*, and anaplastic thyroid tumors *in vivo*. The signal quality achieved with the multi-channel receiver closely matches that achieved with standard commercially available hardware. The receiver is relatively low-cost and is readily integrated into the experimental workflow. This strategy increased throughput, improved experimental efficiency, and reduced the overall cost of these pilot experiments. Investigators that are interested in multi-sample HP measurements such as these can implement a similar receiver system, or provision the configuration of a new or upgraded console with multiple broadband receiver channels.

Despite the dramatic increase in signal afforded by DNP, limited dosage of HP agents to achieve physiologically relevant concentrations results in measurements that remain limited by SNR. For *in vivo* measurement in mice, institutional guidelines for animal care restrict permissible injection volumes to a maximum of 200 μL per injection. To enhance sensitivity and extend the scale of HP experiments, the development of novel RF coils for HP ^{13}C is essential. In the investigation for *in vitro* experiments with the optimized Helmholtz coils to improve SNR and reduce the number of cells for each sample, merely 12.5 μL of the HP agent was injected to maintain a physiologically relevant concentration of lactate and pyruvate in a solution containing a limited number of cells. Experiments with cells required careful coordination of cell preparation and delivery that was synchronized with preparation of HP measurements, and a well-rehearsed process for combining the HP substrate with the cell slurry. Despite the relatively low volume of HP agents, and noise predominantly determined by coil losses in all cases, metabolite time courses were readily measured with sufficient SNR for subsequent analysis. The multi-coil configurations provided improvements in sensitivity and spatial localization, and permitted simultaneous observation of multiple experimental conditions from a single dissolution. The apparent difference in SNR between the two measurements highlighted in Fig. 4 could be the result of bubbles that displaced the cell slurry or variations in the final concentration following rapid manual transfer of such a small volume of HP pyruvate. However, close inspection of the data reveals that the overall SNR between the two measurements is remarkably similar, and that the apparently lower SNR in Fig. 4B is caused by scaling both plots to the maximum value of HP pyruvate seen in each channel. Because cells are exposed to the HP agent for several seconds before the slurry is transferred to coils at isocenter, it is expected that some fraction of HP pyruvate would have been converted into HP lactate even before the first measurement. Thus the initial signal from pyruvate is higher in treated cells, where chemical conversion is seen to be lower; conversely, pyruvate signal is attenuated in the untreated cells, where conversion and initial signal from lactate is higher. In fact the sum total of pyruvate and lactate signals over the whole dynamic measurement, normalized to the standard deviation of noise in each channel, is almost identical.

Although the multi-channel receiver system can be readily scaled to 16 channels (and potentially to 32 channels), up to four-fold throughput improvements were demonstrated in this initial work. Other practical considerations, not related to the receiver, limited the parallelization of experiments. As an example, the location of two flank tumors on a single animal restricted placement of the coils and care was taken to geometrically reduce inductive coupling between coils. We can envision a case where multiple

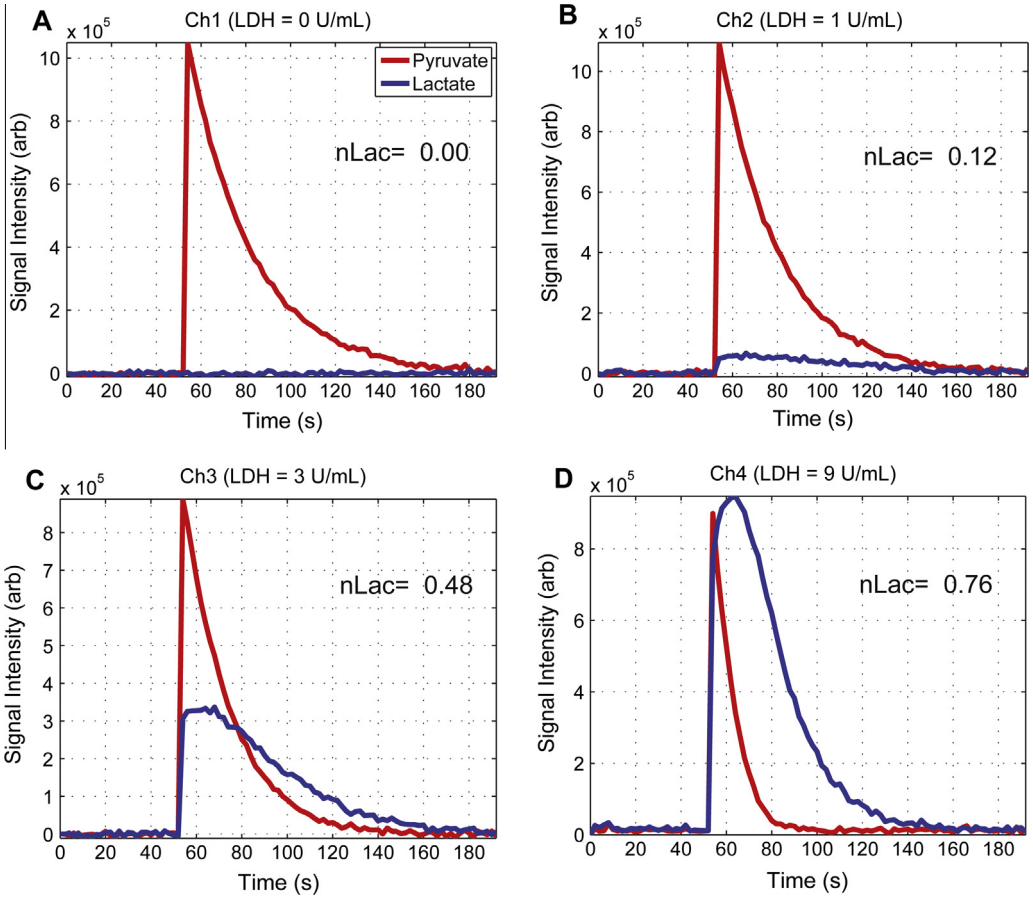

Fig. 3. Simultaneous dynamic measurement of the chemical conversion of HP [1-^{13}C] pyruvate in four distinct samples using a four-channel array. Enzyme phantoms contained different doses of lactate dehydrogenase (LDH) to elicit varying rates of chemical conversion: (A) control: no LDH; (B) 1.0 U/mL; (C) 3.0 U/mL; and (D) 9.0 U/mL. The normalized area under the dynamic lactate curve (nLac) corresponds with LDH concentration.

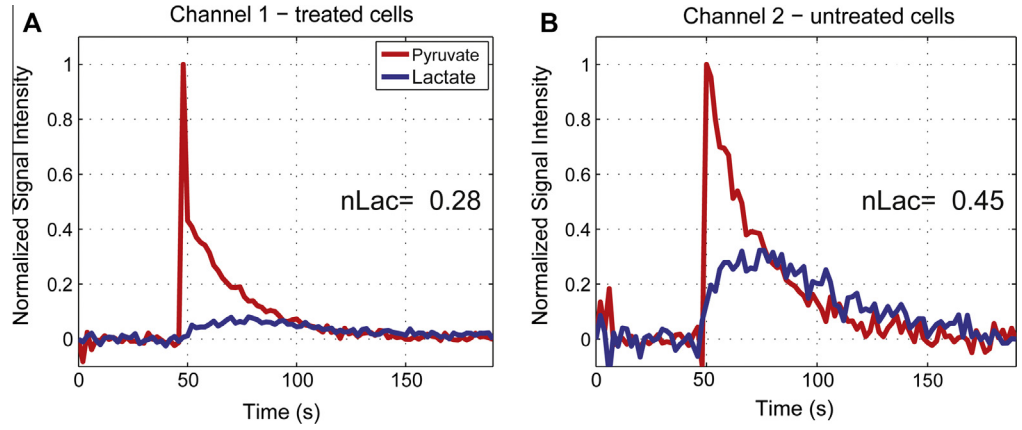

Fig. 4. Simultaneous dynamic conversion of HP pyruvate in anaplastic thyroid cancer cells. (A) cells exposed to 2-deoxyglucose, a competitive inhibitor of glycolysis; (B) untreated control cells. As expected, the relative fraction of HP pyruvate that is converted to lactate is higher in untreated cells.

subcutaneous tumors, with different genotype and/or localized therapy, could be implanted in a single experimental subject. High sensitivity over a large FOV covering multiple regions of interest could be achieved using a more traditional imaging array structure. In imaging applications, such an array would support accelerated imaging strategies [26] and provide important reference information about [1-13C]-pyruvate metabolism in normal tissues and in areas between regions of interest that are known *a priori*. Such arrays also require broadband multichannel receiver capabilities. This work focuses on the use of coil configurations that achieve sufficient spatial localization (via coil sensitivity) to pre-defined experimental geometries for multi-channel dynamic spectroscopy without the need for additional spatial encoding beyond what might have been used in corresponding measurements from a single sample.

Another potential means to improve throughput of *in vivo* measurements is to scan multiple animals simultaneously [31,32]. A preliminary experiment demonstrating this approach

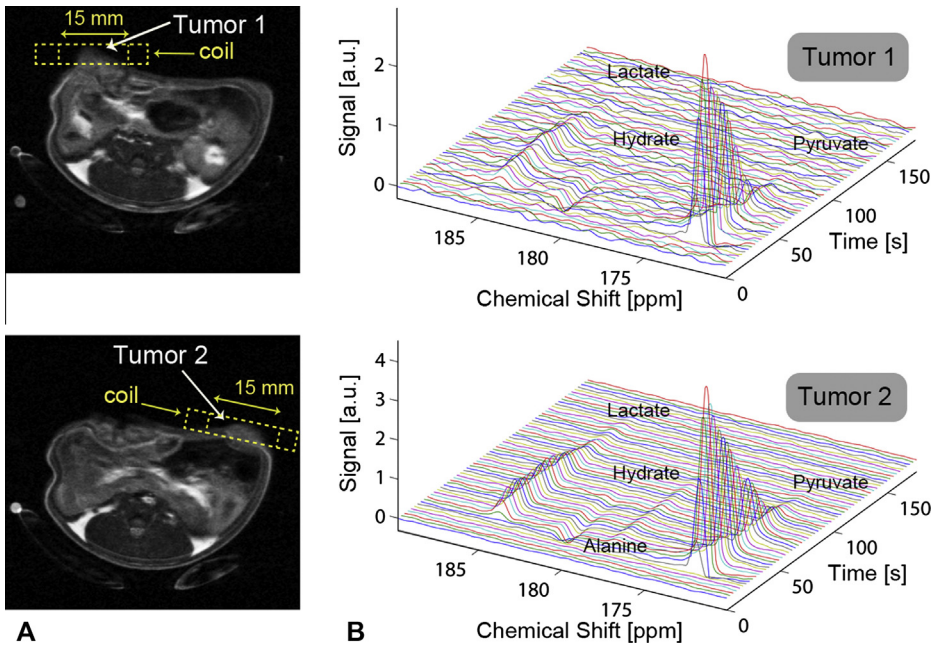

Fig. 5. Simultaneous dynamic measurement of HP pyruvate in two distinct 0805C ATC tumors including approximate locations and sizes of RF coils. (A) The anatomic ^{1}H images show small tumors on the left and right flanks. (B) Dynamic metabolite spectra of tumor 1 (above) and tumor 2 (below) showing time courses of pyruvate (~173 ppm), lactate (~185 ppm), pyruvate–hydrate (~181 ppm), and alanine (~178 ppm).

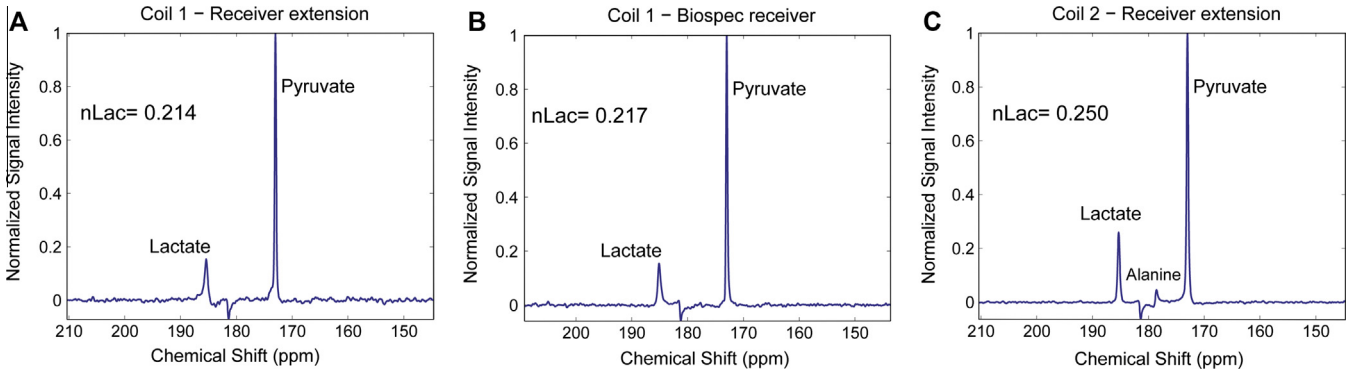

Fig. 6. Temporal sum of dynamic spectra from dual-tumor animal model. The signal from coil 1 was split between (A) the receiver extension and (B) the standard X receive channel for comparison. (C) Coil 2 was placed over "Tumor 2" and signal was detected via receiver extension.

for orthotopic xenografts of ATC, and which leveraged the capability of the receiver developed in this work, was recently presented [33].

Scaling up enzyme or cell experiments is feasible, but will require optimization of larger coil arrays and systems for accurate distribution of substrates to multiple compartments. For the four-channel enzyme phantoms in this work, coils were separated to decrease inductive coupling. This approach required a tradeoff between isolation and shimming performance. This may not be critical for measuring pyruvate and lactate since their chemical shifts are widely separated, but may be necessary when using different ^{13}C label positions or other HP substrates. In this preliminary work, the HP agents were manually delivered into phantoms, cells and animals. Future work will include a robust and repeatable substrate distribution system to improve experimental precision and accuracy. Such a solution should also distribute agents rapidly, since HP signal losses due to T_1 relaxation reduce signal strength. MR-compatible automated injection systems to improve the robustness of injections have been developed [34,35] and can easily be extended to support multiple injections.

Despite the technical challenges that remain, the simultaneous HP detection schemes demonstrated in this work will be crucial to improve the time and cost efficiency for performing biological investigations with high statistical power. Without these strategies, measurements for one experimental time-point from a large cohort of animals may span multiple days, confounding logistical workflow and potentially leading to higher experimental and environmental variations.

In conclusion, a multi-channel acquisition system and purpose-built multinuclear arrays facilitate high-throughput HP ^{13}C investigations. The methods described in this work have the potential to promote the integration of preclinical HP technology into biomedical research to accelerate drug development, improve our understanding of cancer biology, and ultimately lead to discoveries that may be translated into the clinic to improve patient care [36].

Acknowledgments

We thank Charles Kingsley, Jorge de la Cerda, Keith Michel, and Kiersten Maldonado for their support in preparing *in vivo*

experiments at the Small Animal Imaging Facility. This work was supported in part by the National Institutes of Health (P30-CA016672, R21-CA178450) and the Cancer Prevention and Research Institute of Texas (RP101243-P5; RP140021-P5; RP101502; RP140106; RP140113). Funding for C.W. was provided by a Julia Jones Matthews Cancer Research Scholar training award; for M.R. as an Odyssey Fellow by the Odyssey Program and The Estate of C.G. Johnson, Jr; for S.Y. through a CPRIT-CURE Summer Undergraduate Research training award; and for J.L. as a Keck post-doctoral fellow by the W.M. Keck Foundation and the Gulf Coast Consortia.

References

[1] O. Warburg, On the origin of cancer cells, Science 123 (1956) 309–314.
[2] M.G. Vander Heiden, L.C. Cantley, C.B. Thompson, Understanding the Warburg effect: the metabolic requirements of cell proliferation, Science 324 (2009) 1029–1033.
[3] B. Ross, A. Lin, K. Harris, P. Bhattacharya, B. Schweinsburg, Clinical experience with 13C MRS in vivo, NMR Biomed. 16 (2003) 358–369.
[4] R.E. Hurd, Y.-F. Yen, A. Chen, J.H. Ardenkjaer-Larsen, Hyperpolarized 13C metabolic imaging using dissolution dynamic nuclear polarization, J. Magn. Reson. Imaging 36 (2012) 1314–1328.
[5] J.H. Ardenkjær-Larsen, B. Fridlund, A. Gram, G. Hansson, L. Hansson, M.H. Lerche, R. Servin, M. Thaning, K. Golman, Increase in signal-to-noise ratio of >10,000 times in liquid-state NMR, Proc. Natl. Acad. Sci. USA 100 (2003) 10158–10163.
[6] K.R. Keshari, J. Kurhanewicz, R.E. Jeffries, D.M. Wilson, B.J. Dewar, M. Van Criekinge, M. Zierhut, D.B. Vigneron, J.M. Macdonald, Hyperpolarized 13C spectroscopy and an NMR-compatible bioreactor system for the investigation of real-time cellular metabolism, Magn. Reson. Med. 63 (2010) 322–329.
[7] T. Harris, G. Eliyahu, L. Frydman, H. Degani, Kinetics of hyperpolarized 13C1-pyruvate transport and metabolism in living human breast cancer cells, Proc. Natl. Acad. Sci. USA 106 (2009) 18131–18136.
[8] K. Golman, R.I. Zandt, M. Lerche, R. Pehrson, J.H. Ardenkjaer-Larsen, Metabolic imaging by hyperpolarized 13C magnetic resonance imaging for in vivo tumor diagnosis, Cancer Res. 66 (2006) 10855–10860.
[9] K.M. Brindle, S.E. Bohndiek, F.A. Gallagher, M.I. Kettunen, Tumor imaging using hyperpolarized 13C magnetic resonance spectroscopy, Magn. Reson. Med. 66 (2011) 505–519.
[10] T.H. Witney, M.I. Kettunen, D.E. Hu, F.A. Gallagher, S.E. Bohndiek, R. Napolitano, K.M. Brindle, Detecting treatment response in a model of human breast adenocarcinoma using hyperpolarised [1-13C]pyruvate and [1,4-13C2]fumarate, Br. J. Cancer 103 (2010) 1400–1406.
[11] S.E. Bohndiek, M.I. Kettunen, D.E. Hu, K.M. Brindle, Hyperpolarized (13)C spectroscopy detects early changes in tumor vasculature and metabolism after VEGF neutralization, Cancer Res. 72 (2012) 854–864.
[12] S.E. Bohndiek, M.I. Kettunen, D.E. Hu, T.H. Witney, B.W. Kennedy, F.A. Gallagher, K.M. Brindle, Detection of tumor response to a vascular disrupting agent by hyperpolarized 13C magnetic resonance spectroscopy, Mol. Cancer Ther. 9 (2010) 3278–3288.
[13] S.E. Day, M.I. Kettunen, F.A. Gallagher, D.-E. Hu, M. Lerche, J. Wolber, K. Golman, J.H. Ardenkjaer-Larsen, K.M. Brindle, Detecting tumor response to treatment using hyperpolarized 13C magnetic resonance imaging and spectroscopy, Nat. Med. 13 (2007) 1382–1387.
[14] I. Park, R. Bok, T. Ozawa, J.J. Phillips, C.D. James, D.B. Vigneron, S.M. Ronen, S.J. Nelson, Detection of early response to temozolomide treatment in brain tumors using hyperpolarized 13C MR metabolic imaging, J. Magn. Reson. Imaging 33 (2011) 1284–1290.
[15] M.M. Chaumeil, T. Ozawa, I. Park, K. Scott, C.D. James, S.J. Nelson, S.M. Ronen, Hyperpolarized 13C MR spectroscopic imaging can be used to monitor everolimus treatment in vivo in an orthotopic rodent model of glioblastoma, NeuroImage 59 (2012) 193–201.
[16] M.J. Albers, R. Bok, A.P. Chen, C.H. Cunningham, M.L. Zierhut, V.Y. Zhang, S.J. Kohler, J. Tropp, R.E. Hurd, Y.-F. Yen, S.J. Nelson, D.B. Vigneron, J. Kurhanewicz, Hyperpolarized 13C lactate, pyruvate, and alanine: noninvasive biomarkers for prostate cancer detection and grading, Cancer Res. 68 (2008) 8607–8615.
[17] L. Phan, P.C. Chou, G. Velazquez-Torres, I. Samudio, K. Parreno, Y. Huang, C. Tseng, T. Vu, C. Gully, C.H. Su, E. Wang, J. Chen, H.H. Choi, E. Fuentes-Mattei, J. H. Shin, C. Shiang, B. Grabiner, M. Blonska, S. Skerl, Y. Shao, D. Cody, J. Delacerda, C. Kingsley, D. Webb, C. Carlock, Z. Zhou, Y.C. Hsieh, J. Lee, A. Elliott, M. Ramirez, J. Bankson, J. Hazle, Y. Wang, L. Li, S. Weng, N. Rizk, Y.Y. Wen, X. Lin, H. Wang, H. Wang, A. Zhang, X. Xia, Y. Wu, M. Habra, W. Yang, L. Pusztai, S. C. Yeung, M.H. Lee, The cell cycle regulator 14-3-3sigma opposes and reverses cancer metabolic reprogramming, Nat. Commun. 6 (2015) 7530.
[18] V.C. Sandulache, Y. Chen, J. Lee, A. Rubinstein, M.S. Ramirez, H.D. Skinner, C.M. Walker, M.D. Williams, R. Tailor, L.E. Court, J.A. Bankson, S.Y. Lai, Evaluation of hyperpolarized [1-13C]-pyruvate by magnetic resonance to detect ionizing radiation effects in real time, PLoS ONE 9 (2014).
[19] A. Venkatanarayan, P. Raulji, W. Norton, D. Chakravarti, C. Coarfa, X. Su, S.K. Sandur, M.S. Ramirez, J. Lee, C.V. Kingsley, E.F. Sananikone, K. Rajapakshe, K. Naff, J. Parker-Thornburg, J.A. Bankson, K.Y. Tsai, P.H. Gunaratne, E.R. Flores, IAPP-driven metabolic reprogramming induces regression of p53-deficient tumours in vivo, Nature 517 (2015) 626–630.
[20] K. Golman, J.S. Petersson, P. Magnusson, E. Johansson, P. Åkeson, C.M. Chai, G. Hansson, S. Månsson, Cardiac metabolism measured noninvasively by hyperpolarized 13C MRI, Magn. Reson. Med. 59 (2008) 1005–1013.
[21] M.A. Schroeder, L.E. Cochlin, L.C. Heather, K. Clarke, G.K. Radda, D.J. Tyler, In vivo assessment of pyruvate dehydrogenase flux in the heart using hyperpolarized carbon-13 magnetic resonance, Proc. Natl. Acad. Sci. USA 105 (2008) 12051–12056.
[22] E.T. Peterson, J.W. Gordon, M.G. Erickson, S.B. Fain, I.J. Rowland, Dynamic nuclear polarization system output volume reduction using inert fluids, J. Magn. Reson. Imaging 33 (2011) 1003–1008.
[23] B. Wu, Y. Li, C. Wang, D.B. Vigneron, X. Zhang, Multi-reception strategy with improved SNR for multichannel MR imaging, PLoS ONE 7 (2012) e42237.
[24] J. Bodurka, P.J. Ledden, P. van Gelderen, R. Chu, J.A. de Zwart, D. Morris, J.H. Duyn, Scalable multichannel MRI data acquisition system, Magn. Reson. Med. 51 (2004) 165–171.
[25] W. Dominguez-Viqueira, A.Z. Lau, A.P. Chen, C.H. Cunningham, Multichannel receiver coils for improved coverage in cardiac metabolic imaging using prepolarized 13C substrates, Magn. Reson. Med. 70 (2013) 295–300.
[26] M.A. Ohliger, P.E. Larson, R.A. Bok, P. Shin, S. Hu, J. Tropp, F. Robb, L. Carvajal, S. J. Nelson, J. Kurhanewicz, D.B. Vigneron, Combined parallel and partial Fourier MR reconstruction for accelerated 8-channel hyperpolarized carbon-13 in vivo magnetic resonance Spectroscopic imaging (MRSI), J. Magn. Reson. Imaging 38 (2013) 701–713.
[27] P.B. Roemer, W.A. Edelstein, C.E. Hayes, S.P. Souza, O.M. Mueller, The NMR phased array, Magn. Reson. Med. 16 (1990) 192–225.
[28] S.M. Wright, L.L. Wald, Theory and application of array coils in MR spectroscopy, NMR Biomed. 10 (1997) 394–410.
[29] C.M. Walker, J. Lee, M.S. Ramirez, D. Schellingerhout, S. Millward, J.A. Bankson, A catalyzing phantom for reproducible dynamic conversion of hyperpolarized [1-13C]-pyruvate, PLoS ONE 8 (2013) e71274.
[30] V.C. Sandulache, H.D. Skinner, Y. Wang, Y. Chen, C.T. Dodge, T.J. Ow, J.A. Bankson, J.N. Myers, S.Y. Lai, Glycolytic inhibition alters anaplastic thyroid carcinoma tumor metabolism and improves response to conventional chemotherapy and radiation, Mol. Cancer Ther. 11 (2012) 1373–1380.
[31] N.A. Bock, N.B. Konyer, R.M. Henkelman, Multiple-mouse MRI, Magn. Reson. Med. 49 (2003) 158–167.
[32] M.S. Ramirez, S.Y. Lai, J.A. Bankson, A throughput-optimized array system for multiple-mouse MRI, NMR Biomed. 26 (2013) 237–247.
[33] M.S. Ramirez, J. Lee, C.M. Walker, Y. Chen, C.V. Kingsley, J. De La Cerda, K.L. Maldonado, S.Y. Lai, J.A. Bankson, Feasibility of multianimal hyperpolarized (13) C MRS, Magn. Reson. Med. 73 (2015) 1726–1732.
[34] S. Reynolds, S.M. Kazan, J.E. Bluff, M. Port, E. Wholey, G.M. Tozer, M. Paley, Fully MR-compatible syringe pump for the controllable injection of hyperpolarized substrate in animals, Appl. Magn. Reson. 43 (2012) 263–273.
[35] S. Bowen, C. Hilty, Rapid sample injection for hyperpolarized NMR spectroscopy, Phys. Chem. Chem. Phys. 12 (2010) 5766–5770.
[36] S.J. Nelson, J. Kurhanewicz, D.B. Vigneron, P.E. Larson, A.L. Harzstark, M. Ferrone, M. van Criekinge, J.W. Chang, R. Bok, I. Park, G. Reed, L. Carvajal, E.J. Small, P. Munster, V.K. Weinberg, J.H. Ardenkjaer-Larsen, A.P. Chen, R.E. Hurd, L.I. Odegardstuen, F.J. Robb, J. Tropp, J.A. Murray, Metabolic imaging of patients with prostate cancer using hyperpolarized [1-13C]pyruvate, Sci. Transl. Med. 5 (2013) 198ra108.